J. Fluid Mech. (2009), *vol.* 635, *pp.* 171–187.
doi:10.1017/S0022112009007629

Pumping or drag reduction?

JÉRÔME HŒPFFNER† AND KOJI FUKAGATA
Department of Mechanical Engineering, Keio University, Yokohama 223-8522, Japan

(Received 6 August 2008; revised 10 April 2009; accepted 11 April 2009)

Two types of wall actuation in channel flow are considered: travelling waves of wall deformation (peristalsis) and travelling waves of blowing and suction. The flow response and its mechanisms are analysed using nonlinear and weakly nonlinear computations. We show that both actuations induce a flux in the channel in the absence of an imposed pressure gradient and can thus be characterized as pumping. In the context of flow control, pumping and drag reduction are strongly connected, and we seek to define them properly based on these two actuation examples. Movies showing the flow motion for the two types of actuation are available with the online version of this paper (journals.cambridge.org/FLM).

1. Introduction

Aero- and hydrodynamic drag are the main resistances to vehicle motion: airplanes, ships, trains, cars, bicycles... and are thus responsible for a large part of the spent power. This drag usually consists of pressure drag, for instance dramatically increased by flow recirculation, and skin friction drag, dramatically increased by transition to turbulence. Higher speed for lower power can be obtained when the vehicle is designed such as to take advantages of the flow dynamics. Skin friction drag reduction has received much attention: prevention of the transition to turbulence by stabilization of the boundary layer (see, e.g. Joslin 1998; Kim & Bewley 2007) or reduction of the skin friction in the turbulent regime (e.g. Choi, Moin & Kim 1994; Kasagi, Suzuki & Fukagata 2009). The plane channel flow is a simple configuration exhibiting the central elements of skin friction drag (exponential and algebraic instabilities, transition to turbulence, sustained turbulent regime) and was thus used as a test case and a source of inspiration for research in this field.

In view of flow control for drag reduction, it is useful to search for fundamental performance limitations. In Bewley (2001), the following conjecture was proposed (Bewley's conjecture): 'The lowest sustainable drag of an incompressible constant mass flux channel flow, when controlled via a distribution of zero-net mass-flux blowing/suction over the no-slip channel walls, is exactly that of the laminar flow'. A momentum balance in the channel shows that the work of the shear at the walls – acting against the flow – is directly balanced by the work of the pressure at inflow and outflow. As emphasized by Marusic, Joseph & Mahesh (2007), the formulation of the conjecture where the flux is fixed and the pressure gradient is allowed to change, is equivalent to a formulation where the pressure gradient is fixed and the flux is allowed to change. In this case of a fixed pressure gradient, the conjecture tells that

† Email address for correspondence: jerome@fukagata.mech.keio.ac.jp

the actuation cannot induce a flux in excess of the laminar value. In other words whatever the actuation power, the flux cannot be increased.

In Min *et al.* (2006), a blowing and suction boundary condition was applied at the channel walls in the form of a travelling wave in numerical simulations of laminar and turbulent flows; the flux was kept constant by adjusting the pressure gradient for the different actuation parameters: amplitude, wave speed and wavelength. They show that when the wave is made to travel upstream, the fixed flux can be maintained with a lesser pressure gradient than the laminar value, thus achieving sustained sublaminar drag. Their setting complies with the requirement of the conjecture above: constant mass flux, no-slip walls, zero-net mass-flux actuation and sustained drag effect. They thus provide a counter example to Bewley's conjecture.

This result has attracted the attention of Luchini (2006), where a link is drawn between the unexpected sublaminar drag and acoustic streaming. Streaming consists in the generation of a mean drift by an oscillating flow (see Lighthill 1978 for an inspiring lecture and Riley 2001 for a recent review). In his paper, Luchini comes to state 'not drag but thrust', commenting indeed that 'the effect of a zero-mean blowing-and-suction at the wall is not a (multiplicative) influence on the drag-producing mechanism driven by the pressure gradient, but an (additive) pumping that pushes the fluid in one direction or the other independent of any mean pressure gradient applied'. According to Luchini, a travelling wave of blowing and suction at the wall is not drag reduction, it is *pumping*. Luchini has numerically validated this interpretation by showing in his paper that a consistent flow rate could be sustained while turning off the pressure gradient.

We can now turn to the purpose of the present paper. A wide range of phenomena can be categorized as to belonging to the family of streaming, without need of precise considerations on the chain of events leading to the mean drift. We will see through our analysis that subtle effects are at play in the response to the travelling wave actuation. Min *et al.* (2006) close their paper with 'the current control scheme, consisting of surface blowing and suction in the form of travelling waves, is mathematically simple [. . .], yet it may not be straightforward to implement in real flows. [. . .]. However, a moving surface with wavy motion would produce a similar effect, since wavy walls with small amplitudes can be approximated by surface blowing and suction'. On the contrary, we will see that the responses to the two types of actuation – travelling wave of blowing and suction and travelling wave of wall deformation – are very different.

In figure 1 we have represented the velocity fields of the response to the two travelling wave actuations in a plane channel. In both cases, the wave is travelling from left to right. A first intriguing observation is that for the travelling wave of wall deformation, a mean flux is generated to the right – that is, in the same direction as the wave – whereas for the travelling wave of blowing and suction, a mean flux is induced to the left – that is, opposite to the direction of the wave. We will analyse this phenomenon, and distinguish the mechanisms at play.

2. The physics of the travelling wave actuations

2.1. *Travelling wave of wall deformation*

The walls of our channel can now be deformed in the shape of a travelling wave with phase speed c. We can consider the case of sinusoidal waves about the wall original position, or choose a different waveform to emphasize the mechanisms at play. In this first analysis, we consider a channel without imposed mean pressure gradient, i.e. no Poiseuille profile. Impact of the mean pressure gradient will be estimated in the

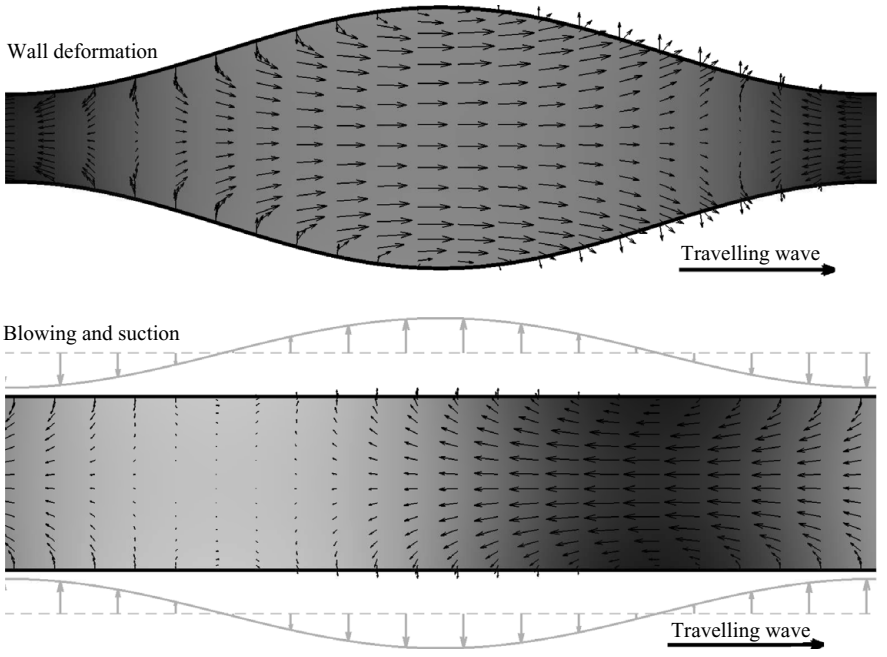

FIGURE 1. Velocity and pressure fields in the peristalsis and blowing/suction cases, the Reynolds number is 300, wave amplitude is $\phi = 0.5$, and the wavelength is $L = 6$. The pressure field is indicated by grey shading: lowest pressure is black. The flow motion is best viewed from the movies available with the online version of this paper (journals.cambridge.org/FLM).

appendix. The system quantities are made dimensionless with respect to the channel half height h, fluid density ρ, viscosity μ and wave speed c. The Reynolds number relevant for this analysis is then defined as $Re_w = \rho ch/\mu$. We parametrize the wall wave amplitude with ϕ, the maximum displacement of the walls from $y = \pm 1$. That is, $\phi = 0$ means a straight channel and $\phi = 1$ implies a deformation such that the channel is occluded. Hereafter, the direction of the wave propagation and its opposite will be termed, respectively, the forward and the backward directions. Note that particles at the wall only move in the vertical direction, while the wave of deformation propagates in the horizontal direction, that is, no forward motion is imposed at the wall.

When travelling in the frame of the wave, the flow has steady boundary conditions and a fixed domain. It can thus be computed as a stationary solution of the Navier–Stokes equations in the domain deformed with the waveform. The Navier–Stokes equations are discretized in space using the fourth-order finite differences, with no-slip boundary conditions at the displaced walls and periodicity in the horizontal direction. The steady-state flow is computed using the Newton method.

The pumping mechanism has a viscous origin. Propagation of the deformation induces a flow from regions being constricted to regions being expanded. Without viscosity, this flow would be equally distributed to the forward and backward directions: no pumping. The backward flow takes place in a constricted channel, whereas the forward flow takes place in an expanded channel. For a viscous fluid, the larger friction in the constricted region induces an asymmetry in favour to the forward flow, thus a mean flux in the direction of the propagation of the wave: this is the pumping mechanism. The flux will be small when the wall deformation is

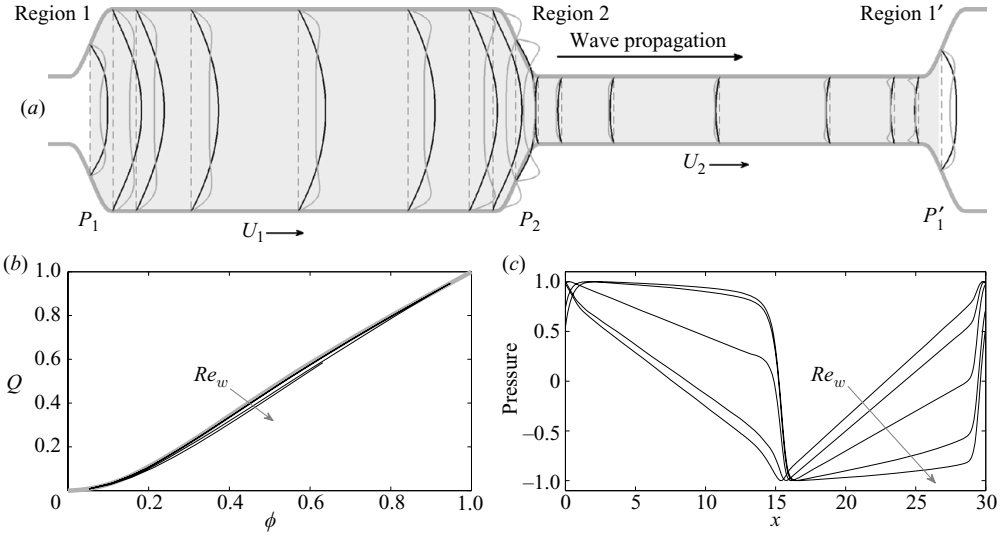

FIGURE 2. Configuration of peristaltic pumping model (2.6). (*a*) Velocity profiles for $\phi = 0.5$, wavelength $L = 30$ and $Re_w = 1$ (black) and $Re_w = 1000$ (light grey). For $Re_w = 0.1, 1, 10, 100, 1000$, (*b*) pressure along one wavelength, normalized to the amplitude range $[-1, 1]$.

small, and reach a maximum when the channel is occluded, at $\phi = 1$. In this limit, the trapped flow is forced forward at the speed of the wave; the flux is unity.

For low Reynolds numbers, long wavelength and sinusoidal wall deformation, a closed-form expression for the flux can be derived from the Stokes equation: $Q_{sin} = 3\phi^2/(2 + \phi^2)$ (Jaffrin & Shapiro 1971). For the purpose of illustrating the mechanism at play, we wish to derive an equivalent expression directly from the above description of the mechanism. A good qualitative match with the computed data will thus be a confirmation of the understanding of the mechanism. With this aim, we take the freedom to change the flow geometry so that the key effects clearly appear. The pumping results from different head losses in the forward and backward flows. A waveform which emphasizes this mechanism consists of short constrictions and expansions that connect long sections of straight channel, as shown in figure 2. The wave of wall deformation propagates from left to right, thus, region 1 is a zone where the channel is being constricted, whereas region 2 is a zone where the channel is being expanded. This effect is clearly visible in the movies. The pressure at the constriction region 1 and expansion region 2 are denoted by P_1 and P_2. There is no externally imposed mean pressure gradient, thus the pressure P_1' in the region $1'$ is equal to P_1.

The flow motion originates from the displacement of the wall deformation. Conservation of mass in a fixed control volume enclosing region 2 being expanded accounts for this effect: the ingoing flux F_1 on the left of region 2 plus the ingoing flux $-F_2$ on the right equals the rate of increase of volume of the region. This change of volume is 2ϕ, because of an height expansion of 2ϕ at unit speed. This gives

$$F_1 - F_2 = 2\phi. \tag{2.1}$$

To obtain a second relation for F_1 and F_2 we impose that the total pressure rise must be zero over one wavelength; this condition imposes that the skin friction in the

constricted channel be equal in amplitude and opposite in sign to the skin friction in the expanded channel

$$\frac{\partial u_1}{\partial y}|_{wall} + \frac{\partial u_2}{\partial y}|_{wall} = 0. \tag{2.2}$$

We assume Poiseuille profiles in both channel sections

$$u_1 = U_1[1 - y^2/(1+\phi)^2], \quad u_2 = U_2[1 - y^2/(1-\phi)^2],$$

where we have accounted for the different half height $1+\phi$ and $1-\phi$ in the expanded and constricted channels. From these expression, we can obtain the expression of the skin friction in each channel, which with (2.2) leads to

$$(1-\phi)^2 U_1 + (1+\phi)^2 U_2 = 0. \tag{2.3}$$

The flux is the integral of the velocity profile over the channel

$$F_1 = 2U_1(1+\phi)/3, \quad F_2 = 2U_2(1-\phi)/3. \tag{2.4}$$

The total flux of the pumping is

$$Q = \frac{1}{L}\int_{x=0}^{L} F(x)\,\mathrm{d}x = \frac{1}{L}\left(\frac{L}{2}F_1 + \frac{L}{2}F_2\right) = (F_1 + F_2)/2, \tag{2.5}$$

where L is the wavelength. Combining (2.1), (2.3), (2.4) and (2.5), we finally obtain the expression for Q as a function of ϕ

$$Q = \phi\frac{(1+\phi)^3 - (1-\phi)^3}{(1+\phi)^3 + (1-\phi)^3}. \tag{2.6}$$

It vanishes for straight channel ($\phi = 0$), grows quadratically at low ϕ, and tends to unity for occlusion ($\phi = 1$). The computed velocity profiles are shown in figure 2. The computed flux is compared to that obtained from (2.6), which shows excellent agreement. The pressure along the channel centreline is also represented for several Reynolds numbers.

It is remarkable that the flux does not depend on the Reynolds number. Viscosity is essential for this pumping mechanism: the competition of viscous resistance in the constricted and expanded channels. But this competition appears as a ratio of the contribution of each section, thus the Reynolds number disappears. We will see in § 4 on the other hand that the energy spent does depend on the Reynolds number.

The details of the flow about the constriction and expansion regions have little effect at long wavelengths, thus their exact shape is immaterial to the pumping. At low Reynolds numbers, the centreline pressure has a typical Poiseuille shape, with a constant slope opposed to the flow direction. For larger Reynolds numbers, large pressure gradients are concentrated in the short regions of flow acceleration and deceleration, which is a typical inviscid limit behaviour.

In figure 3, we have represented the trajectories of five particles during six periods of the travelling waves. Flow particles follow a circular motion with a mean drift to the right.

2.2. *Travelling wave of blowing and suction*

We now let the channel walls rest at $y = \pm 1$, but blowing and suction is imposed as the boundary condition on the vertical velocity. For the horizontal velocity, no-slip condition applies. Once again, the flow is steady in the frame travelling with the wave, and can be computed with the same tools as for § 2.1 using finite differences and the Newton method.

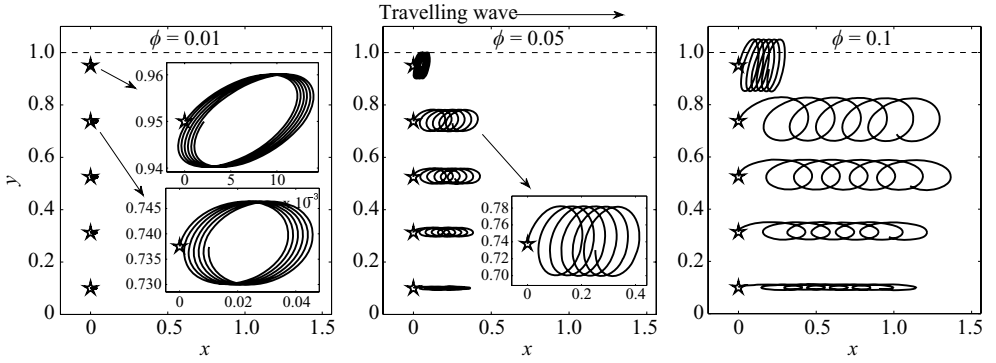

FIGURE 3. Trajectories of five particles at $Re_w = 100$, $L = 10$ for six periods. Stars locate the particles' initial position. The motion of flow particles is shown in the movies available with the online version of this paper.

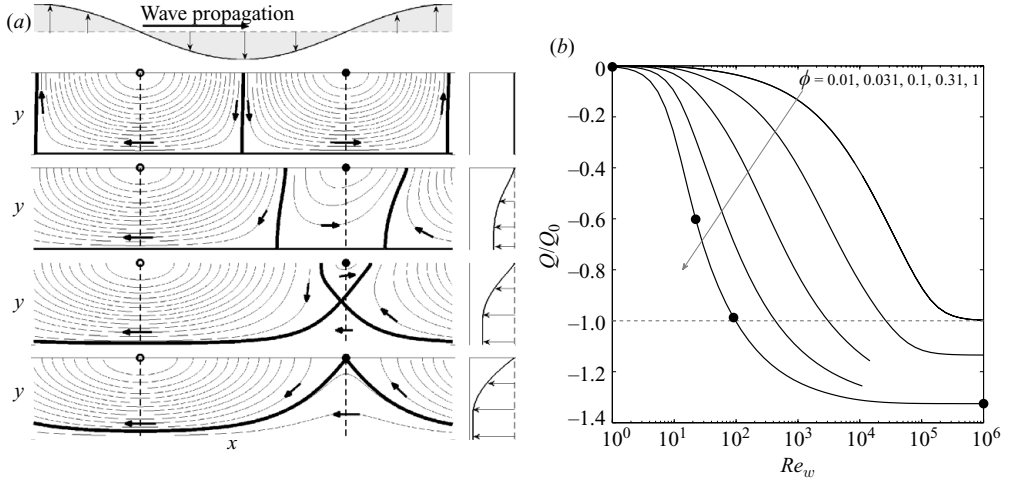

FIGURE 4. Travelling wave of blowing and suction. (*a*) Instantaneous streamlines and averaged streamwise profile in the upper half of the channel for $\phi = 1$ at Reynolds corresponding to the black dots of (*b*). (*b*) Mean flux normalized by $|Q_0|$ as a function of the Reynolds number for five different ϕ values.

Instantaneous streamlines in the frame at rest are shown in figure 4(*a*) while increasing the Reynolds number; the upper half of the channel is represented. At low Reynolds numbers, the flow is structured in two cells of equal length, each one corresponding to the inflow/outflow of fluid particles at the walls due to the boundary condition. One cell corresponds to particles flowing forward, the other cell corresponds to particles flowing backward. When the Reynolds number is raised – which can be thought as progressively increasing the wave speed – the forward cell shrinks to the advantage of the backward cell.

Changes in the relative sizes of the forward and backward cells are a kinematic consequence of the dynamic effects at play in the pumping mechanism. The total flux Q is the average over one wavelength of the local flux $F(x)$

$$Q = \frac{1}{L}\int_{x=0}^{x=L} F(x)\,\mathrm{d}x. \tag{2.7}$$

Since the flux between two streamlines is a constant, the streamline pattern connects the flux in the domain to the flux at the boundaries, which is imposed and known. Equal lengths of the two cells imply that half of the flux injected at the wall is directed forward and half of the flux injected at the wall is directed backward: zero pumping. When on the other hand, the forward cell shrinks, more of the flow injected at the walls is gathered to the backward direction: negative pumping.

For large Reynolds number, the forward cell vanishes. At the Reynolds number where the forward cell just disappears, assuming that all streamlines start or end at the walls, the total flux can be quantified as

$$Q_0 = \frac{1}{L}\int_{x=0}^{L} \underbrace{\int_{\xi=0}^{x} -\eta(\xi)\,\mathrm{d}\xi}_{F(\xi)}\,\mathrm{d}x = \frac{1}{L}\int_{0}^{L} x\eta(x)\,\mathrm{d}x,$$

where η is the waveform. For a sinusoidal η, the integration gives $Q_0 = -\phi L/2\pi$. This result is a gross evaluation of the maximum flux; it conveys the physics of the structuring of the streamline pattern into two cells and the disappearing of the forward cell.

The mean flux computed while varying the wave amplitude and the Reynolds number is shown in figure 4(*b*), normalized by Q_0. The flux is negative (backward), and increases in amplitude with Reynolds number until reaching a constant value. We observe that the maximum flux is larger than Q_0; indeed, streamlines that are not connected to the wall inflow/outflow are present. These correspond to particles in the centre region, entrained by the near-wall flow motion.

It remains now to penetrate the dynamic processes at play. To this end, it is helpful to switch to a Lagrangian flow description. For a stationary wave ($c = 0$), particles follow trajectories from inflow regions to outflow regions. In this cell structure, up/down and forward/backward displacements are synchronized into a convection structure, as seen in figure 4(*a*). Here, since the wave speed is zero, trajectories are superposed on the streamlines; all particles emanate from the wall and are eventually sucked back.

When the wave is set to travel, the streamline convection structure is maintained. Some particles still enter and exit through the walls, but there will also be particles that remain in the channel. They are advected up and down as suction and blowing zones travel nearby at the wall, and they are also advected forward and backward in a synchronized manner. The motion can be imagined by translating rightward the streamline patterns of figure 4, letting the particles velocity be tangent to the instantaneous streamlines. Let us now follow one such particle, initially at distance y_0 from the wall. It is convected close to the wall and back to y_0 through the forward part of its motion, then away from the wall and back to y_0 in the backward part of its motion. In the absence of fluid viscosity, this sequence would form a closed loop: after one period, the particle returns to its initial position. For a viscous fluid on the other hand, particle motion being hindered close to the wall due to the no-slip condition, an asymmetry results in favour of the backward motion: after one period of the travelling wave, our particle returns to y_0 but has moved a finite distance in the backward direction. The synchronization of vertical and horizontal displacements is best viewed in the movies available with the online version of this paper.

Particle trajectories in the frame at rest are shown in figure 5 for three wave amplitudes. For the lowest amplitude, the circular trajectories have small radius. A zoom shows a slight backward drift. For the larger wave amplitudes, the particles

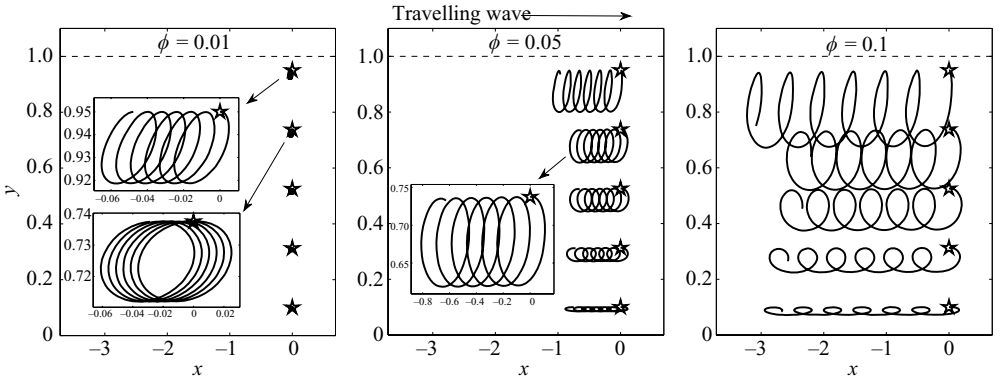

FIGURE 5. Trajectories of five particles at $Re_w = 100$, $L = 10$ for six periods, with three wave amplitudes $\phi = 0.01, 0.05, 0.1$. Stars locate the particles' initial position. The motion of flow particles is shown in the movies available with the online version of this paper.

show clearly the trend described above, with a damped forward motion, leading to a rapid drift.

Variation of the Reynolds number introduces an additional phenomenon. For low Reynolds numbers, slow-down of particles due to the no-slip walls influences the complete domain, thus both forward and backward motions are affected though with slightly different magnitude: low pumping. At large Reynolds numbers, bulk inertia of particles in the centre of the channel dominates and the no-slip boundary condition is felt only in a thin viscous layer close to the wall. The particles that will contribute most to the pumping are those that oscillate about the edge of this viscous layer: flowing freely when outside (backward), and nearly stopped when penetrating (forward).

2.3. *Pumping efficiency*

We will now consider the spent power for peristalsis and blowing and suction. The energy budget is composed on one hand of viscous dissipation, and on the other hand, of the work of the actuation. At steady state, the total energy is constant in time. For blowing and suction, energy is injected through the work of the pressure at the wall

$$\text{Blowing and suction:} \quad W_{act} = -\overline{v(p + v^2/2)}|_{y=1}$$

energy is transferred from the actuation to the fluid if the top wall pressure has its sign opposite to the sign of the velocity v. Note that here, as for the definition of the flux, we consider only the top half of the channel. For peristalsis, wall deformation induces a contribution of viscous forces

$$\text{Peristalsis:} \quad W_{act} = -\overline{v_n(p + E_K)}|_{wall} + \frac{1}{Re_w}\overline{\frac{\partial E_K}{\partial n}}|_{wall},$$

where v_n is the velocity normal to the wall, and $\partial E_K/\partial n$ is the normal derivative of the kinetic energy, with $E_K = (u^2 + v^2)/2$. In this expression, the overline $\bar{\cdot}$ denotes average along the top wall. For more details on these expressions, see for instance Mito & Kasagi (1998). If an external pressure gradient P_x is present, there is an other source for energy

$$\text{Pressure gradient:} \quad W_{pg} = -\frac{1}{L}\int_{xy} u P_x \, \mathrm{d}x \, \mathrm{d}y = -Q P_x.$$

Energy is injected to the flow if P decreases in the direction of the flux.

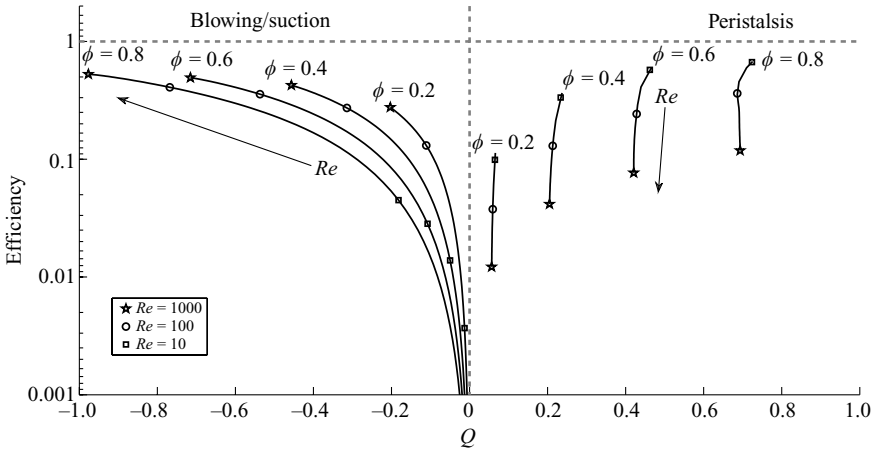

FIGURE 6. Flux and efficiency of pumping while varying the Reynolds number $Re_w \in [1, 1000]$ (solid line), and the actuation amplitude ϕ, for $L = 2\pi$. Note that the case $Re_w = 1$ is not represented by an additional symbol.

We now seek to define a pumping efficiency. Let us suppose that a given flow actuation induces a flux Q in absence of an external pressure gradient. This actuation can be said efficient if the needed energy is close to the energy needed to drive the same flux with only an external pressure gradient (laminar Poiseuille flow). The pressure gradient needed to drive a Poiseuille flow of flux Q is $P_x^{ref} = -3Q/Re_w$, thus the reference power is

$$\text{Reference:} \quad W_{ref} = -Q P_x^{ref} = 3Q^2/Re_w.$$

The efficiency can then be defined as the reference power divided by the total injected power; this leads to

$$\text{Efficiency} = \frac{W_{ref}}{W_{act} + W_{pg}} = \frac{3Q^2}{Re_w} \frac{1}{W_{act} + W_{pg}}.$$

Note that this efficiency must be unity whenever $W_{act} = 0$. In figure 6, we show how the efficiency depends on the Reynolds number and actuation amplitude ϕ. Here, $W_{pg} = 0$.

We observe that the efficiency is always less than one, namely, it always costs more energy to drive a given flux with the travelling wave actuation than with a pressure gradient. The most notable information here is that for blowing and suction, efficiency increases with Re_w, whereas for peristalsis, efficiency is best at lowest Reynolds number. For the computations presented here, the overall best efficiency is found for peristalsis: about 0.73 at lowest Reynolds number ($Re_w = 1$) and at highest actuation amplitude ($\phi = 0.8$).

3. Flow control

The drag reduction problem was formulated in Bewley (2001) as finding the lowest power for a given flux Q in the channel. It was conjectured that *whatever* the actuation power W_{act}, it is impossible to use a pressure gradient power less than the laminar value $3Q^2/Re$; Min *et al.* (2006) gave a counter example.

Clearly, the actuation power must be accounted for when searching for a performance limitation in flow control. In Fukagata, Sugiyama & Kasagi (2009),

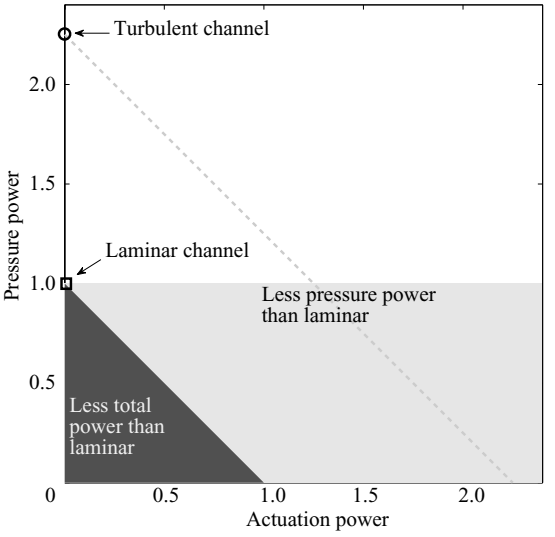

FIGURE 7. The power plane. Open square: power for laminar Poiseuille; open circle: power for turbulent Poiseuille. Powers are normalized with that needed to drive the laminar Poiseuille flow. Light grey: less pressure power than laminar, dark grey: less total power than laminar.

a lower bound is demonstrated for the power spent by the work of the pressure gradient plus the power spent by the actuation. This total power injected into the flow must balance the only cause of damping: viscous dissipation in the flow domain (see also Bewley in press). The flow motion which for a given set of boundary conditions experiences the least viscous damping is that satisfying the Stokes equation. It is interesting that precisely the flow where viscosity dominates is the one which dissipates least. The channel is a parallel geometry such that inertial effects do not affect its steady state in the laminar regime; the parabolic profile is solution to the Stokes equation, it is therefore the ideal drag reduction target.

We have represented in figure 7 the different zones of interest. This is the 'power plane'. At zero actuation power, there are two possible sustained regimes: laminar (square) or turbulent (circle). Powers are normalized with that needed to drive the laminar Poiseuille flow. Here, the power required to drive the turbulent flow is slightly more than twice that of the laminar case. This corresponds to the turbulent simulations in Min *et al.* (2006) at Reynolds number 2000. The oblique paths in this graph correspond to constant total driving power. Two regions are highlighted: the shaded strip is the domain forbidden by Bewley's conjecture: whatever the actuation energy, one cannot drive a given flux with less pressure power than that of the laminar flow. The dark triangle is the domain forbidden by Fukagata *et al.* (2009): one cannot drive a given flux with less total power than that of the laminar flow.

Presented as here, figure 7 emphasizes for the pressure power, in the spirit of Bewley's conjecture. Now that it is clear that the total power must be considered, it is more relevant to orient the axis such that horizontal lines correspond to total power. We have performed this change in figure 8. Here the axes of the previous figure are rotated 45° and scaled accordingly. We have, here again, highlighted the forbidden zone where the power is less than laminar.

We would like now to place the travelling wave actuation in this diagram. In this section, we are interested in large Reynolds numbers, that is, in a parameter range

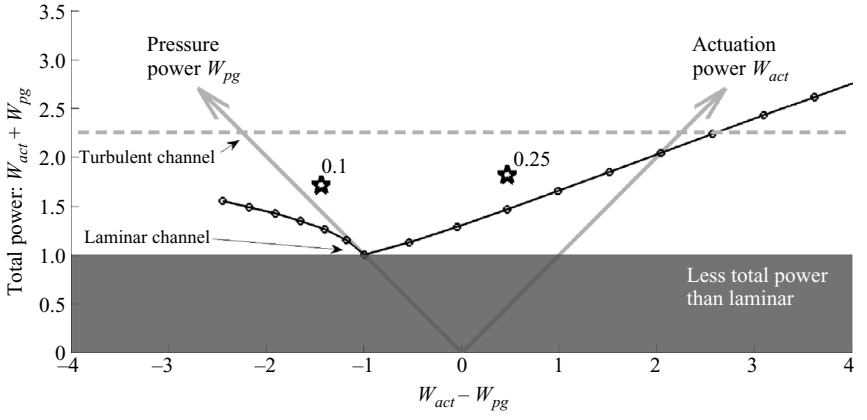

FIGURE 8. An alternative representation of the 'power plane'. Here the axes are rotated such that horizontal lines correspond to constant total power $W_{act} + W_{pg}$. The dotted line represents the power balance for blowing and suction for a fixed flux Q, at $Re_w = Re_c = 2000$. The two stars are the turbulent control results of Min *et al.* (2006) with wave amplitudes 0.1 and 0.25.

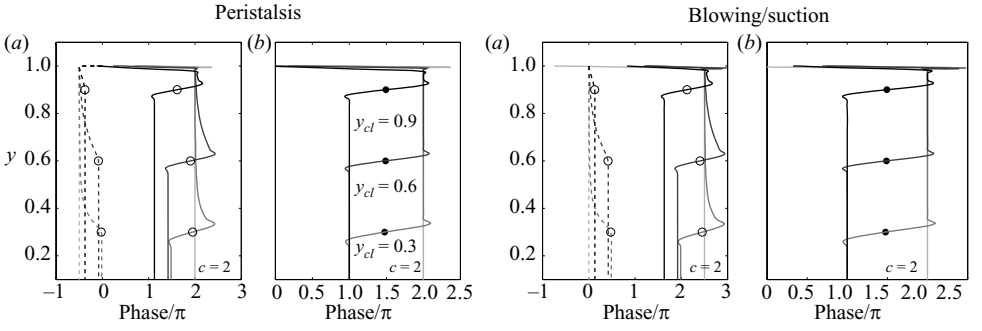

FIGURE 9. (*a*) Phase of $\hat{u}_y$ (plain), $\hat{v}$ (broken) and (*b*) departure from quadrature: $\text{phase}(\hat{u}_y) - \text{phase}(\hat{v}) - \pi/2$, at $Re_c = 10^6$ for $c = 2$ (light grey), and for wave speeds such that the critical layers are at $y_{cl} = 0.3, 0.6, 0.9$ (from grey to black). The position of the critical layer is shown with the symbols.

where the peristaltic pumping is inefficient. We thus only consider the travelling wave of blowing and suction. We are now interested in the case of a fixed flux $Q = 2/3$. This flux corresponds to a centreline velocity $U_c = 1$, thus here $Re_w = Re_c = 2000$. We keep a wavelength of $L = 2\pi$ with a wave speed of unity $c = \pm 1$. We vary the wave amplitude and adjust the pressure gradient accordingly in order to maintain $Q = 2/3$. We can then compute the pressure and actuation power, and report it on the diagram. The results are shown in figure 8.

We observe as expected that the total power is always larger than that of the laminar Poiseuille. We have also considered the case of negative pressure power, that is when the actuation power is too large, and must be compensated by an adverse pressure gradient to maintain the desired flux. The case where actuation power is negative has also been considered: the wave is made to travel downstream and pumps against the flux, which is compensated with a large pressure power in favour of downstream flux.

We now examine the case of the travelling waves in Min *et al.* (2006) for the turbulent regime. The pressure gradient and actuation powers for waves of amplitudes 0.1 and 0.25 are shown by the two stars of figure 8. The mechanism at play in this

turbulent case is of great interest. Indeed, the total power is reduced as compared to the turbulent flow without actuation. We have in the preceding sections analysed the physics of the pumping effect in the laminar case, and care must be taken when extrapolating our observation to a regime of a great complexity. We can nevertheless state a safe comment: there is drag reduction in the turbulent regime; power is not simply transferred from pressure gradient pumping to actuation pumping. To explain this effect, Luchini (2006) suggests that suction regions absorb turbulent flow whereas blowing regions inject laminar flow, resulting in a global decrease of the turbulence intensity, wall normal mixing and thus drag. A turbulent channel with constant suction at one wall and constant blowing at the other wall should have this effect. This test was performed in Fukagata, Iwamoto & Kasagi (2002), but in fact it results in an increased drag, thus discarding this mechanism as a potential explanation of Min's results.

We can now build on the observations of the present paper to suggest a mechanism that interestingly links drag reduction to pumping. It is here a temptative mechanism, which we only could assess if supported by critical scrutiny of turbulent flow data. At first, the upstream travelling wave of wall actuation induces a flux in the downstream direction. In the context of a channel with constant flux, this effect results in a lower pressure gradient: this is the pumping effect. Fukagata *et al.* (2002) have analysed the drag reduction effects in turbulent channels, and have shown the central role played by the Reynolds stress. They show that the pressure gradient is proportional to the spatial average of $yu'v'$ – that is, the Reynolds shear stress weighted with the distance from the centreline. Naturally, the decrease of the Reynolds shear stress due to the lowered pressure gradient in turn leads to a decrease of the turbulence production. At last, there is a decrease of turbulent mixing caused by the decrease of the turbulent production: this is the drag reduction effect.

4. Conclusion

Travelling waves of wall deformation induce pumping in the forward direction. On the other hand, travelling waves of blowing and suction induce pumping in the backward direction. In both cases, fluid particles are entrained into a circular motion by the wall actuation; in both cases the pumping direction originates from a different viscous damping during the backward and forward motion of fluid particles along its circular trajectory. For peristalsis, the particles' backward motion takes place in the constricted section of the channel, where viscosity slows down the flow. For blowing and suction, the particles' forward motion takes place close to the walls, where viscosity slows down the flow.

A weakly nonlinear analysis, as done in the appendix, provides a different point of view. The leading-order solution in both cases is a zero mean motion of the same order of amplitude as the wall actuation. The Reynolds shear stress generated by this leading-order solution acts as a forcing to the second-order solution, being balanced by viscous forces. This induces a creeping flow with a net flux, from which a backward pumping originates, as observed for the blowing and suction case. For peristalsis an additional effect is present: a non-zero boundary condition on the second-order solution due to quadratic interaction of the leading-order solution and the wall deformation. This additional effect acts opposite to the Reynolds stress effect, inducing forward pumping.

The question of flow control in the channel can be formulated in two equivalent ways: for a given flux, how can we reduce the required amount of energy? or

equivalently for a given amount of energy, how can we increase the flux? The first formulation is usually preferred since it is common to define the Reynolds number based on the laminar centreline velocity or bulk-mean velocity. The two equivalent formulations for the motion of a vehicle are: for a given speed, how can we reduce the driving power? or, for a given driving power, how can we increase the reachable speed? As emphasized in Bewley & Aamo (2004), the performance should be reached, but also sustained.

It is usual to drive a flux in a channel by imposing an external pressure gradient, for instance with a differential inlet/outlet pressure or a body force. One can also induce a flux using a localized pump, for instance a powered propeller inserted in the channel. The flux will be hindered by viscous effects until a balance is found between the skin friction and the power injected through the propeller. Of course, one would not be tempted to categorize an externally powered propeller as a drag reduction device, even though the total flux is increased for a given pressure gradient, or the required pressure gradient for a given flux is decreased: this propeller is a pumping device.

In a pipe or a channel, *pumping* is an action that induces a flux in the absence of any other injected power. Applying a pressure gradient is pumping, inserting a powered propeller is pumping, applying travelling waves of wall deformation or blowing and suction is pumping. Now, for a given pumping, *drag reduction* is an action such that the total power to drive the same flux is reduced, or equivalently, the flux obtained by a given total power is increased. For vehicles, pumping becomes *thrust* and induces a motion in absence of any other source of energy, whereas drag reduction results in less power for the same speed or a larger speed for the same power.

It is shown in Fukagata *et al.* (2009) that the parabolic flow profile in the channel is that leading to the least viscous damping. Any actuation that disturbs the flow from this profile shall increase the required power; namely, drag reduction is impossible when the base flow is the Poiseuille flow. The pumping efficiency – defined as the ratio of the energy dissipated by the Poiseuille profile over the total injected energy – must be lower than or equal to one. It is on the other hand possible to achieve drag reduction from the turbulent regime, since the flow is then not a solution of the Stokes equations. The example of turbulent drag reduction of Min *et al.* (2006) might be understood as a secondary effect of pumping, as discussed in § 3. Based on this discussion, we advocate the representation of flow control results in the form of the 'power plane' of figure 8. This graphical representation emphasizes the total input power as a central feature of the performance.

Appendix. Weakly nonlinear analysis

We can gain yet an alternative point of view on the mechanisms if we assume small amplitude actuation. We will see that the first-order solution does not lead to flux, and obtain a diffusive equation for the second-order solution, whose average in x does not vanish. This setting will also be useful to study how the presence of a Poiseuille base flow can lead to specific phenomena.

A.1. *Boundary conditions*

We consider the case of small amplitude wall deformation/blowing and suction, where we can decompose the response with respect to the different orders of its magnitude. This analysis can be done in the weakly nonlinear framework. We will see that the leading-order solution will induce an oscillatory motion, particles following circular

trajectories about a fixed point, and that a mean drift will be induced at second order, responsible for the pumping, in the forward direction for wall displacement, and in the backward direction for blowing and suction. This framework will also be useful to investigate the effect of an imposed pressure gradient, a case where a mean Poiseuille flow profile is present. The Reynolds number is now defined as $Re_c = \rho U_c h/\mu$, based on the channel half height h, channel centreline velocity U_c, fluid density ρ and viscosity μ.

We perform an amplitude expansion of flow quantities

$$u = U + \varepsilon u' + \varepsilon^2 u''/2 + O(\varepsilon^3), \tag{A 1}$$

where ε is a small amplitude parameter. By introducing these amplitude expansions for u, v and p in the Navier–Stokes equation, we find that U is the parabolic profile induced by the external pressure gradient, and u', v', p' obey the Navier–Stokes equation linearized about U. The pumping effect appears from the streamwise average of the second-order amplitude solution u'', which obey the equation

$$\frac{1}{Re_c}\overline{u''_{yy}} = \overline{v'u'_y}, \tag{A 2}$$

where the subscript y denotes derivative in the vertical direction, and the overline denotes equivalently average in time over one period, or average in space over one wavelength.

Denoting by η the actuation waveform, the boundary conditions of the blowing/suction case are $u = 0, v = \varepsilon\eta$, of amplitude ε. Therefore, all boundary conditions are zero, except $v' = \eta$. For peristalsis, the no-slip condition at the displaced walls can be expanded to $y = \pm 1$, since the wall displacement $\varepsilon\eta$ is small

$$u_{|_{1+\varepsilon\eta}} = 0 = u_{|_1} + \varepsilon\eta\, u_{y|_1} + \frac{(\varepsilon\eta)^2}{2} u_{yy|_1} + O(\varepsilon^3).$$

We can now inject our amplitude expansion (A 1) in this expression, here for u at the top wall

$$\begin{aligned} u|_{1+\eta} = 0 = &\left[U + \varepsilon u' + \tfrac{\varepsilon^2}{2}u''\right]_{|_1} \\ &+ \varepsilon\eta\, \left[U_y + \varepsilon u'_y + \tfrac{\varepsilon^2}{2}u''_y\right]_{|_1} \\ &+ \tfrac{(\varepsilon\eta)^2}{2}\left[U_{yy} + \varepsilon u'_{yy} + \tfrac{\varepsilon^2}{2}u''_{yy}\right]_{|_1} + O(\varepsilon^3). \end{aligned}$$

We see from this expression that the double expansion (in amplitude and in space about $y = \pm 1$) induces interactions between the solutions of different orders at the walls. We now gather like orders of ε. We obtain zero boundary conditions on U; for the first-order amplitude solution, we have $u' + \eta U_y = 0$, $v' = \eta_t$, thus there is a non-zero boundary condition on the streamwise velocity – depending on the base shear – and v' equals the time derivative of the waveform. At second order, $\overline{u''} = \overline{\eta u'_y}$: a non-zero boundary condition (slip velocity) resulting from the quadratic interaction of the leading-order solution and the wall displacement.

If the external pressure gradient is set to zero, we have $U = U_y = 0$ and the boundary conditions become

$$\begin{array}{lllll} \text{Peristalsis:} & u'|_{\pm 1} = 0, & v'|_{\pm 1} = \eta_t, & \overline{u''}|_{\pm 1} = \overline{\eta u'_y}|_{y=\pm 1}, \\ \text{Blowing/suction:} & u'|_{\pm 1} = 0, & v'|_{\pm 1} = \eta, & \overline{u''}|_{\pm 1} = 0. \end{array} \tag{A 3}$$

This set of boundary conditions, together with (A 2), is most representative of the differences and similarities between the two types of actuation. The first-order solution

(u', v') obeys in both cases the dynamics of a wave of blowing and suction. Through (A 2), this first-order solution induces a forced creeping flow: a pumping proportional to the Reynolds number. We found through our computation that this effect was always favourable to backward pumping: both for peristalsis and blowing/suction. For peristalsis only, the quadratic interaction of the first-order solution and the wall displacement $\overline{\eta u'_y}$ result in a slip velocity for the second-order solution, which we found to be always favourable to forward pumping, and its effect always dominate the backward pumping due to the Reynolds stress term.

We now consider a sinusoidal waveform

$$\eta = \cos[\alpha(x - ct)] = [e^{i\alpha(x-ct)} + e^{-i\alpha(x-ct)}]/2,$$

with α the wavenumber and $i = \sqrt{-1}$. With this parametrization, the wavelength is $L = 2\pi/\alpha$. The zeroth-order solution U is a Poiseuille profile, constant in x. The first-order solution satisfies the Navier–Stokes equations linearized about U, with boundary conditions based on η. The first-order solution is thus only composed of the fundamental frequency: it has the same periodicity as η and can thus be written as

$$u'(x, y, t) = [\hat{u}(y)e^{i\alpha(x-ct)} + \hat{u}(y)^* e^{-i\alpha(x-ct)}]/2,$$
$$v'(x, y, t) = [\hat{v}(y)e^{i\alpha(x-ct)} + \hat{v}(y)^* e^{-i\alpha(x-ct)}]/2;$$

here, $\hat{u}$ and $\hat{v}$ are complex functions of y, whose complex arguments represent the y-dependent horizontal phase shift with respect to the waveform imposed at the wall. Here, $*$ denotes the complex-conjugate. We can now express the averaging $\overline{v'u'_y}$ of (A 2) in terms of the complex amplitude functions

$$\overline{v'u'_y} = \frac{1}{L}\int_0^L (\hat{v}\hat{u}_y e^{2i\alpha(x-ct)} + \hat{v}^*\hat{u}_y^* e^{-2i\alpha(x-ct)} + \hat{v}\hat{u}_y^* + \hat{v}^*\hat{u}_y)/4\,dx = \text{real}(\hat{v}\hat{u}_y^*)/2.$$

This result implies that the pumping effect originating from the Reynolds stress term in (A 2) vanishes whenever v and u_y are in phase quadrature ($\hat{v}\hat{u}_y^*$ is purely imaginary). Conversely, any departure from phase quadrature induces pumping.

The second pumping effect, which is present only for peristalsis comes from the slip boundary condition on $\overline{u''}$, at $y = 1$ for instance

$$\overline{\eta u'_y} = \text{real}(\hat{u}_y)/2;$$

this pumping effect disappear whenever if u'_y is in phase quadrature with η (i.e. $\hat{u}_y$ is purely imaginary); conversely, departure from quadrature induces pumping.

A.2. *Base flow effect: critical layers*

We are now interested in the pumping effect if in addition to the wall actuation, there is an external pressure gradient inducing a Poiseuille flow. The weakly nonlinear framework is ideal to investigate the interaction between the base flow profile and the actuation. In Min *et al.* (2006), a large drag increase is observed if the wall wave is made to travel downstream. We will see that this effect is due to the presence of critical layers.

When a wave of constant amplitude propagates on a shear, locations of the base flow at which the velocity equals the wave speed play a special role. These are *critical layers*. In the inviscid limit, a critical layer corresponds to a singular point of the linear dynamic equations. When viscosity is present, this singularity is smoothed, but its effect is still felt, increasingly for large Reynolds numbers (see Maslowe 1986). Here, we have two critical layers whenever $c \in [0, 1]$, at $y = \pm\sqrt{1 - c}$. They are just

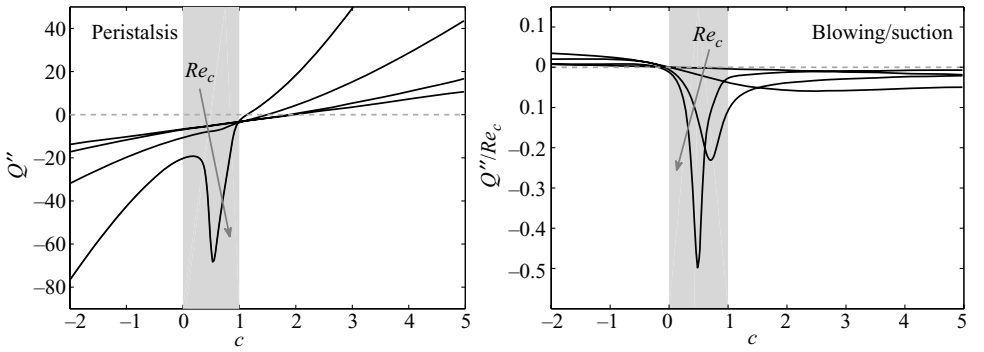

FIGURE 10. Wall actuation interaction with base flow: pumping flux as a function of the wave speed c for $Re_c = 1, 10, 100, 1000$. The parameter range where a critical layer is present $c \in [0, 1]$ is highlighted by a shaded strip.

at the walls for $c = 0$ and merge in the centre at $c = 1$. In the low-amplitude limit, the streamfunction is known to go through a phase change of π across the critical layer. This effect is visible in figure 9, where c was chosen such as to have critical layers at $y = \pm 0.3, \pm 0.6, \pm 0.9$. It is interesting to note that for both peristalsis and blowing/suction, the critical layer effect ($c \in [0, 1]$) always opposes the Poiseuille flow, thus acting such as to reduce the flux for a given pressure gradient.

Another location where $\hat{u}_y$ and $\hat{v}$ depart from quadrature is close to the walls in two thin viscous layers. In the absence of critical layers, the pumping effect for the blowing and suction case is entirely induced by this near-wall viscous effect: a phase lag of $\hat{u}_y$ due to the no-slip boundary condition. The impact of the presence of the critical layer can be seen in figure 10, where the obtained flux is shown while varying the speed c of the travelling wave actuation. This critical layer effect is clearly opposed to the base flow flux (negative Q″).

We note that Mittra & Prasad (1974) have analysed the interaction of peristalsis with Poiseuille flow, but have considered low Reynolds number relevant for biological applications where the effect of critical layers is small.

The authors are grateful to Dr Shinnosuke Obi (Keio University) and Dr Nobuhide Kasagi (The University of Tokyo) for fruitful discussions. This work was supported through Grant-in-Aid for JSPS Fellows (19-07821) as well as Grant-in-Aid for Scientific Research (A) by Japan Society for the Promotion of Science (JSPS).

REFERENCES

BEWLEY, T. R. 2001 Flow control: new challenges for a new renaissance. *Prog. Aerospace Sci.* **37**, 21–58.

BEWLEY, T. R. 2009 A fundamental limit on the balance of power in a transpiration-controlled channel flow. *J. Fluid Mech.* **632**, 443–446.

BEWLEY, T. R. & AAMO, O. M. 2004 A 'win-win' mechanism for low-drag transients in controlled two-dimensional channel flow and its implications for sustained drag reduction. *J. Fluid Mech.* **499**, 183–196.

CHOI, H., MOIN, P. & KIM, J. 1994 Active turbulence control for drag reduction in wall-bounded flows. *J. Fluid Mech.* **262**, 75–110.

FUKAGATA, K., IWAMOTO, K. & KASAGI, N. 2002 Contribution of Reynolds stress distribution to the skin friction in wall-bounded flows. *Phys. Fluids* **14**, L73–L76.

Fukagata, K., Sugiyama, K. & Kasagi, N. 2009 On the lower bound of net driving power in controlled duct flows. *Phys. D*. **238**, 1082–1086.

Jaffrin, M. Y. & Shapiro, A. H. 1971 Peristaltic pumping. *Annu. Rev. Fluid Mech.* **3**, 13–37.

Joslin, R. D. 1998 Aircraft laminar flow control. *Annu. Rev. Fluid Mech.* **30**, 1–29.

Kasagi, N., Suzuki, Y. & Fukagata, K. 2009 Microelectromechanical systems-based feedback control of turbulence for skin friction reduction. *Annu. Rev. Fluid Mech.* **41**, 231–251.

Kim, J. & Bewley, T. R. 2007 A linear systems approach to flow control. *Annu. Rev. Fluid Mech.* **39**, 383–417.

Lighthill, Sir J. 1978 Acoustic streaming. *J. Sound Vib*. **61** (3), 391–418.

Luchini, P. 2006 Acoustic streaming and lower-than-laminar drag in controlled channel flow. In *Progress in Industrial Mathematics at ECMI*, Mathematics in Industry, vol. 12, pp. 169–177. Springer.

Marusic, I., Joseph, D. D. & Mahesh, K. 2007 Laminar and turbulent comparisons for channel flow and flow control. *J. Fluid Mech.* **570**, 467–477.

Maslowe, S. A. 1986 Critical layers in fluid mechanics. *Annu. Rev. Fluid Mech.* **18**, 405–432.

Min, T., Kang, S. M., Speyer, J. L. & Kim, J. 2006 Sustained sub-laminar drag in a fully developed channel flow. *J. Fluid Mech.* **558**, 309–318.

Mito, Y. & Kasagi, N. 1998 DNS study of turbulence modification with streamwise-uniform sinusoidal wall-oscillation. *Intl J. Heat Fluid Flow* **19**, 470–481.

Mittra, T. K. & Prasad, S. N. 1974 Interaction of peristaltic motion with Poiseuille flow. *Bull. Math. Biol.* **36**, 127–141.

Riley, N. 2001 Steady streaming. *Annu. Rev. Fluid Mech.* **33**, 43–65.